RESEARCH ARTICLE | SEPTEMBER 18 2024

Hollow cylindrical three-dimensional nonlinear photonic crystal for annular beam generation

Ruonan Wang ; Qiang Cao ; Xiaoliang Wang; Fengchang Li

Appl. Phys. Lett. 125, 121113 (2024)
https://doi.org/10.1063/5.0219725

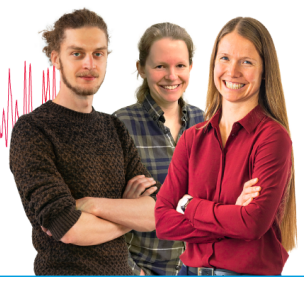

Applied Physics Letters ARTICLE pubs.aip.org/aip/apl

Hollow cylindrical three-dimensional nonlinear photonic crystal for annular beam generation

Cite as: Appl. Phys. Lett. **125**, 121113 (2024); doi: 10.1063/5.0219725
Submitted: 19 May 2024 · Accepted: 9 September 2024 ·
Published Online: 18 September 2024

View Online Export Citation CrossMark

Ruonan Wang, Qiang Cao,[a] Xiaoliang Wang, and Fengchang Li

AFFILIATIONS

The Institute of Technological Sciences, Wuhan University, Wuhan 430072, China

[a]Author to whom correspondence should be addressed: caoqiang@whu.edu.cn

ABSTRACT

We present a hollow cylindrical three-dimensional nonlinear photonic crystal for annular beam shaping. By inducing a modification with the near-infrared femtosecond laser inside lithium niobate, we experimentally achieve second-order nonlinear optical coefficient modulation in three dimensions. The center dark spot ratio of the generated annular beam can be adjusted by varying the hollow ratio of the cylindrical structure. To demonstrate the controlled linear variation of the annular distribution, we generate annular beams with center dark spot ratios ranging from 0 to 0.7. Furthermore, we illustrate the feasibility of the generated annular beam in optical trapping by manipulating glass powder particles with diameters of 4–10 μm in water. Our hollow cylindrical structure owns effective control of beam dark spot ratio, while providing a tool for generating annular beam.

The annular beam is a structured light beam whose amplitude distribution is characterized by a central aperture and toroidal radiation. It can be used in optical trapping,[1–3] optical communication,[4] quantum computing, and quantum cryptography.[5,6] The linear generation of annular beam adjusts the phase and amplitude of the incident beam by special optical elements (e.g., diffractive optics,[7] spatial light modulators,[8,9] phase plates,[10,11] metamaterials[12]). In contrast, nonlinear beam shaping has the advantage of simultaneous frequency conversion and beam intensity transformation, yet its related research is still very limited. Nonlinear photonic crystal (NPC), which realizes a quasi-phase matching (QPM) process by periodically spatially varying the second-order nonlinear optical coefficients [$\chi(2)$], has received attention for nonlinear annular beam shaping.[13–15] However, most previous works on one- and two-dimensional (2D) NPC suffer from low conversion efficiency.

The near-infrared femtosecond laser spatially modulated $\chi(2)$ technique is used to fabricate three-dimensional (3D) NPC. This approach opens up new avenues for improving the nonlinear conversion efficiency.[16–19] Compared to 2D NPC, 3D NPC provides an extra dimension to ensure that the quasi-phase matching condition is satisfied. Currently, there are two main structures of 3D NPC for annular beam shaping: One is the 3D fork grating NPC obtained by binary computer-generated hologram theory.[20,21] For example, Wei *et al.* fabricated a 3D fork grating NPC in lithium niobate using a femtosecond laser. This resulted in a two-order-of-magnitude improvement in the conversion efficiency of nonlinear beam shaping compared to the 2D case.[22] Another approach involves the utilization of the 3D helical NPC based on nonlinear volume holography theory.[23,24] The concept of second harmonic (SH) beam shaping using a helical nonlinear structure was demonstrated by Imbrock *et al.*[25] However, the complex cross section structure of the 3D NPC remains challenging. Femtosecond laser processing has relatively low optical resolution along the depth direction. Additionally, the use of motorized stages in the processing system can introduce errors when fabricating continuously varying smooth structures. As a result, 3D NPC structural errors are usually more severe than those of low-dimensional NPCs. This may disrupt the phase matching of the NPC and prevent it from realizing the desired nonlinear optical function.

To simplify the fabrication process of 3D NPC and reduce manufacturing errors, Liu *et al.* proposed a discretized structure consisting of four units.[26] The generalized simplified structure addresses the fabrication challenges associated with complex 3D structures, while preserving the functionality of pre-designed 3D NPC. However, as the topological charge of the annular beam increases, the complexity of the structure and the number of corresponding discretization units also increase. Reducing the manufacturing difficulty requires adopting a larger sampling period, yet this approach still faces the potential issue of disrupting the phase matching of the NPC. The center dark spot ratio, denoted as "c," represents the ratio between the inner and outer diameters of the beam. It reflects the proportion of the center dark

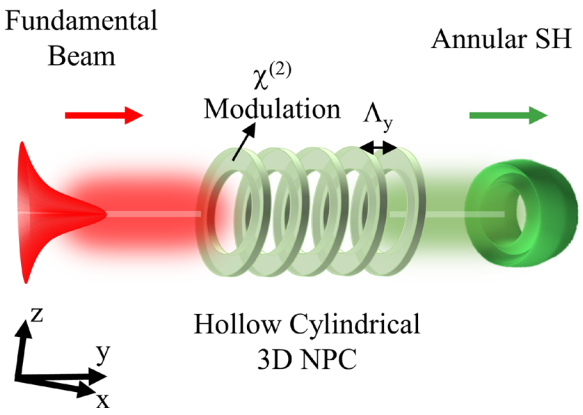

FIG. 1. Design principle of 3D hollow cylindrical NPC. The generated annular SH intensity highly depends on the QPM mechanism. The conversion efficiency is affected by the interaction length.

spot size to the beam width, serving as a significant characteristic parameter of the annular beam. Therefore, it is necessary to provide the 3D NPC structure that is easy to fabricate to enable the generation of annular beam with larger center dark spot ratio.

Here, we design the 3D hollow cylindrical NPC for annular beam shaping. By inducing a modification with the near-infrared femtosecond laser inside lithium niobate, we achieve $\chi(2)$ modulation in three dimensions. This enables adjustable variations in the center dark spot ratio of the annular beam by manipulating the hollow ratio of the cylindrical structure.

The structural design principle of the 3D hollow cylindrical NPC is shown in Fig. 1. The design principle applies only to the undepleted-pump approximation condition. The interaction length of the QPM grating determines the intensity and efficiency of the second harmonic generation. Therefore, a periodic QPM grating structure can be used. This principle has been applied to fabricate a 3D conic NPC, experimentally extending the nonlinear Gaussian to flat-top beam shaping from 1D to 2D.[29] Its cross-sectional spatial second-order nonlinear optical coefficients can be modulated into a toroidal distribution. This enables the transformation of the annular SH intensity distribution. In the region without periodicity, the SH conversion efficiency is negligible. The outer diameter of the annular cross section is aligned with the given pump beam profile. The incident fundamental beam propagates along the y-axis perpendicular to the polar axis, z, of the crystal. The fundamental beam (red beam in Fig. 1) has a Gaussian distribution. After passing through the 3D NPC, the SH (green beam in Fig. 1) can obtain an annular distribution. By adjusting the hollow ratio of the cylindrical structure, a controllable variation of the dark spot region at the center of the annular beam can be achieved.

We experimentally fabricated 3D hollow cylindrical NPC inside a z-cut 5% MgO-doped lithium niobate crystal. A representative femtosecond laser writing system was used for our fabrication process. The light source is a femtosecond-pulsed laser (pulse width, 190 fs; repetition rate, 200 kHz) from a regenerative amplified laser system based on Yb:KGW at a wavelength of 1026 nm. Sample movement is controlled by a high-precision displacement holder equipped with a PC-driven three-axis XYZ cross-roller bearing positioning system, with a spatial resolution of 1 nm. The laser is focused by a 50× microscope objective (NA = 0.42) and the spot size at the processing focal plane is approximately 1 μm. During processing, the femtosecond laser is polarized along the x-direction of the crystal. Maintaining the overall homogeneity of the structure is essential for the preparation of 3D NPC. In order to compensate for focal spot distortion caused by aberrations and absorption losses, the pulse energy needs to be adjusted with increasing depth. The pulse energy is continuously adjusted by an attenuator consisting of a half-wave plate and a polarizing plate. Starting at a depth of 120 μm below the crystal +z surface, 20 layers are processed upward. The pulse energies for the top and bottom layers are 2.5 and 10 μJ, respectively. The scanning speed is 100 μm s^{-1}.

Figure 2 depicts the characterization of the laser-processed 3D NPC. Figures 2(a) and 2(d)–2(k) are observed by Čerenkov-type SH confocal microscope (FVMPE-RS, Olympus). The excited SH is enhanced by Čerenkov-type effects at the boundary of second-order nonlinear fluctuations, which is the theory of this nondestructive characterization.[30] Figure 2(a) shows the partial 3D cylindrical NPC generating an annular beam with a center dark spot ratio of 0.7. The xz-plane annular cell has an outer diameter of 100 μm, and its characteristic end is depicted in Fig. 2(b). Radial sections of the NPC generating annular beams with center dark spot ratios ranging from 0 to 0.7 are shown in Figs. 2(d)–2(k). According to the QPM conditions, the fundamental beam wavelength is 1030 nm with a period of $\Lambda_y = 6.3$ μm. The duty cycle is 1/6.3. The modified region exhibits a clear periodic structure with uniform morphology. The NPC hollow region expands as the central dark spot ratio increases. Figure 2(c) displays micro-Raman signals of the processed and unprocessed regions. The processed region exhibits a notably weaker Raman signal, suggesting a significant decrease possibly caused by physical structural changes.[16] According to the Raman spectrum, the depletion rate is 0.275. The modification of the femtosecond laser pulse leads to a change in the $\chi(2)$ and refractive index of the crystal. By measuring the intensity of the center spot and the intensity of the nonzero-order diffracted spot,[27] we calculated the change in refractive index to be about 8×10^{-3}.

Next, the Gaussian to annular beam shaping is performed. We used a laser beam reduction system for a 100 μm spot diameter pump beam. It includes a concave lens (focal length 15 mm) and a convex lens (focal length 750 mm). The fundamental beam has a wavelength of 1030 nm, pulse duration of 270 fs, and repetition frequency of 100 kHz. The y-axis of the sample is set in the direction of propagation of the input light, and the z-axis is set in the vertical direction. A CCD camera is used for image acquisition. The SH emitted by the crystal is expanded by a 4× beam expander. Data are acquired by the CCD at a 100 mm distance from the crystal's emitting end. For power measurements, the CCD is replaced by a power meter with a 0.1 μW resolution accuracy. The pump light is independently incident on the 3D NPC of Figs. 2(d)–2(k).

Figure 3 shows the theoretical and experimental normalized intensity distributions of the SH beam at pump power 0.1 mW. Figures 3(a)–3(h) display the annular SH with center dark spot ratios ranging from 0 to 0.7. The experimentally obtained SH intensity matches the corresponding simulated distribution. Non-uniform SH intensity conversion results in less symmetric and regular intensity distribution for the annular SH. Figure 4(a) displays the normalized intensity along the horizontal pixel line (marked by white dashed line in Fig. 3). Similarly, Fig. 4(b) shows the normalized intensity along the vertical pixel line (marked by white solid line in Fig. 3).

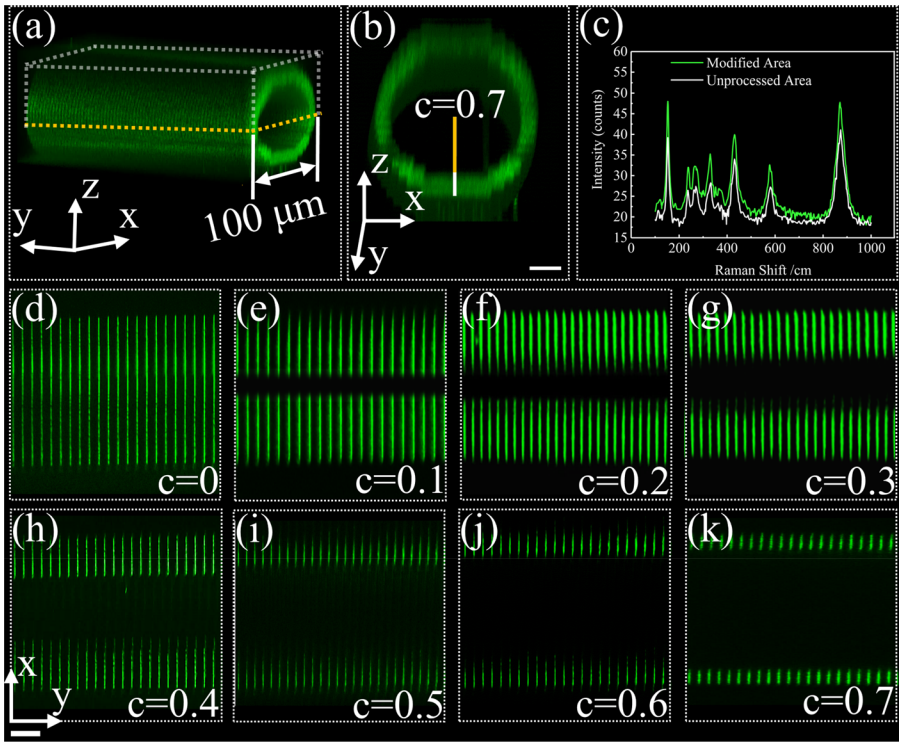

FIG. 2. Characterization of the partial 3D NPC (scale bar length: 20 μm). The total length of the QPM grating is 630 μm. (a) Partial 3D cylindrical NPC for generating annular beam (center dark spot ratio c = 0.7). (b) Front view of the NPC. (c) Micro-Raman signal of the processed area and unprocessed area. (d)–(k) Radial sections [xy-planes marked by yellow dashed line in (a)] of NPCs for generating annular beam with varying center dark spot ratio.

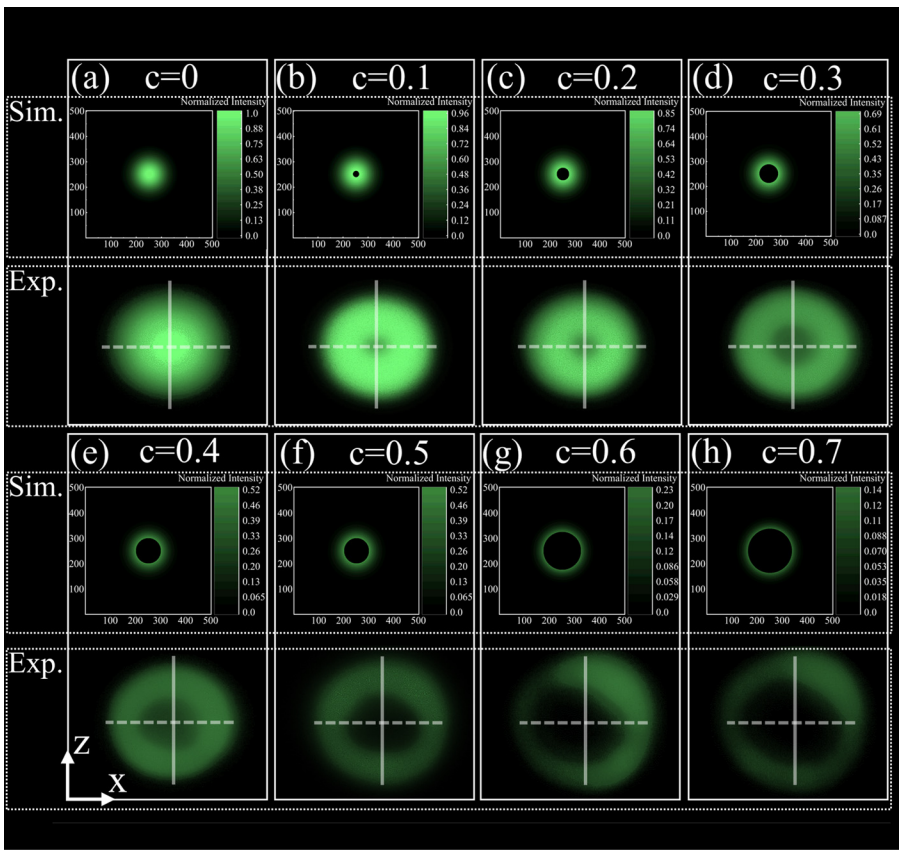

FIG. 3. The theoretical and experimental normalized intensity distributions of the SH beam at pump power 0.1 mW. (a)–(h) Annular SH with center dark spot ratios ranging from 0 to 0.7.

The theoretical peak intensities for annular SH (center dark spot ratios: 0.1–0.7) are 0.961, 0.850, 0.695, 0.521, 0.368, 0.237, and 0.140. The experimentally acquired average peak intensities along the horizontal direction (average of two peaks) are 0.863, 0.779, 0.575, 0.383, 0.260, 0.081, and 0.047, based on Fig. 4(a). Along the vertical direction, the values are 0.825, 0.759, 0.540, 0.406, 0.250, 0.096, and 0.063, as seen in Fig. 4(b). The experimental values of c for annular SH beams (theoretical c: 0.1–0.7) are 0.0997, 0.1986, 0.2884, 0.3625, 0.471, 0.6325, and 0.6827 horizontally, and they are 0.1131, 0.1904, 0.2903, 0.3794, 0.4507, 0.6259, and 0.6704 vertically. The value of c is closer to 1, indicating a larger size of the annular dark spot. Slight deviations from theoretical values are due to minor refractive index changes caused by laser-induced modifications in lithium niobate. However, these errors are within an acceptable range and do not affect the agreement between experimental and theoretical values.

Figure 4(c) shows the relationship between annular SH power and pump power. The effective nonlinearity is 0.223 pm/V. The simulated curve closely matches experimental results [based on Eq. (7) of the supplementary material in Ref. 22]. At pump power 1 mW (peak power $\approx$ 37 kW), the conversion efficiency of c = 0.3 annular SH is approximately 1.07×10^{-2}. Given the low conversion efficiency, small-signal approximation suffices. The neglect of group-velocity dispersion is justified by taking into account the magnitude of the interaction length. Increasing QPM length, fundamental input energy, and adjusting duty cycle contribute to improving the conversion efficiency.[19] The duty cycle can be adjusted by changing the scanning step size in laser processing. Minor refractive index variations affect conversion efficiency in our experiment. A portion of the energy in the central part of the pump beam is not used for second harmonic generation. The extent of wasted pump energy is closely tied to the center dark spot region of the target beam. It is essential to consider the specific circumstances and select an appropriate center dark spot ratio. Furthermore, fabricating periodic circular structure (corresponding to the structure with center dark spot ratio c = 0) with appropriate interaction length before or after the hollow structure can improve the nonlinear conversion efficiency in the central part of the pump beam. Additionally, the multibeam scheme that superimposes or couples an annular beam with a Gaussian beam, which distributes the energy between the different beams, might also be a good option of compensation. Figure 4(d) shows the relationship between simulated and measured SH powers and fundamental wavelength at input an power of 0.75 mW with temperature 20 °C.[28]

We optically manipulated glass powder particles (diameters 4–10 μm) using an annular beam (c = 0.5). The annular beam is focused by a 10× microscope objective (NA = 0.26) and the spot size at the focal plane is approximately 10 μm. Figure 5 illustrates the optical capture process acquired by a color camera. The particle remains confined within the beam despite distortion caused by scattering, partial reflection, and interference when the beam is focused inside the water. In Fig. 5(a), the particle is enveloped by the annular beam at the location indicated by the white dashed circle. By moving the displacement stage in the negative x-axis direction, the particle, bound by the beam, moves in the positive x-axis direction relative to the substrate on the stage [as indicated by the white arrow in Fig. 5(a)]. Following displacement, the particle resides at the position denoted by the white

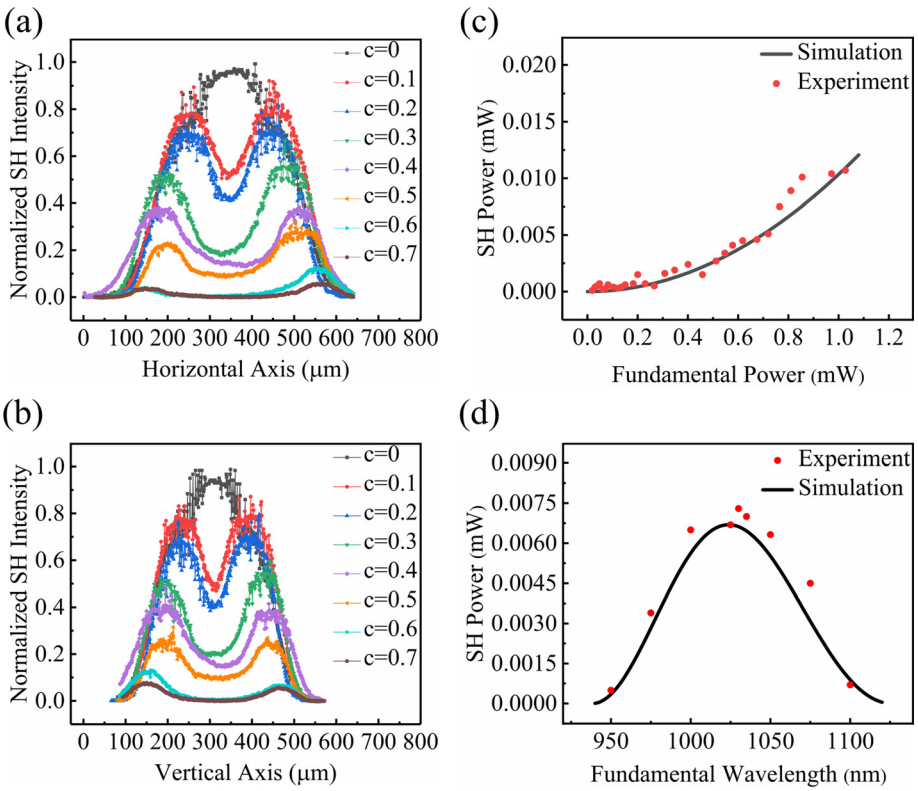

FIG. 4. (a) and (b) Normalized intensity slices through the generated SH beams, obtained from a single line of pixels of the CCD camera at the spot center. (a) Along the x-axis (corresponding to the dashed white lines in Fig. 3). (b) Along the z-axis (corresponding to solid white lines in Fig. 3). (c) Output c = 0.3 SH powers after beam shaping vs pump power at QPM wavelength of 1030 nm. At a pump power of 1 mW, the SH power reaches 0.0107 mW. (d) SH power dependence on fundamental wavelength when the pump power is 0.75 mW.

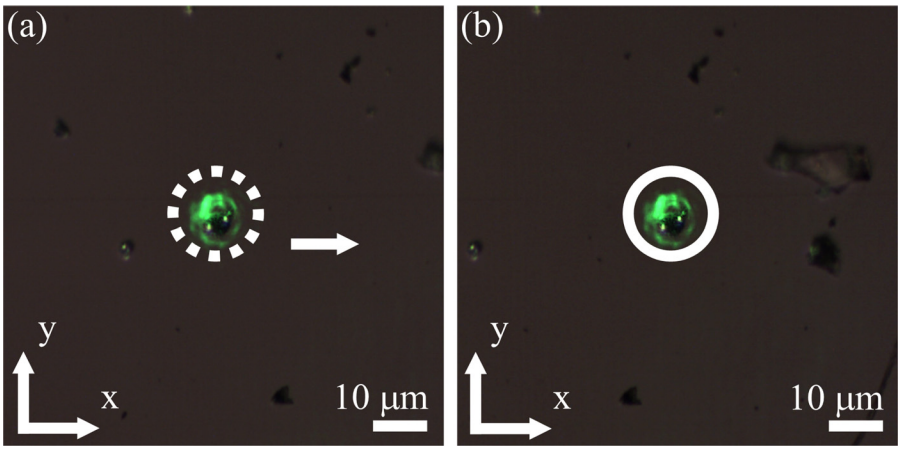

FIG. 5. Optical manipulation of glass powder particles (diameters 4–10 μm) using an annular beam (c = 0.5). (a) Before relative displacement. (b) After relative displacement (the white scale bar length: 10 μm).

solid circle on the substrate, as shown in Fig. 5(b). Due to limited trapping force relative to sample weight, the z-direction manipulation time was too short. We were unable to record effective manipulation in the depth direction.

In conclusion, we have designed and fabricated a 3D hollow cylindrical nonlinear photonic crystal for generating annular beam. The 3D hollow cylindrical nonlinear photonic crystal modulates the pump beam only in amplitude and not in phase. We have experimentally achieved annular beams with adjustable dark spot ratios (0–0.7), demonstrating controllable linear variations. The experimentally obtained annular second harmonic intensity matches the corresponding simulated distribution. Achieving the ideal annular second harmonic with a value of c equal to 1 is not feasible. Additionally, the feasibility of optical trapping with the generated annular beam has been demonstrated by manipulating glass powder particles (diameters 4–10 μm) in water. There are still some areas that need further improvement, such as the lack of rotational freedom in optical manipulation and mitigating group velocity mismatch effects. In this work, effectively control the generated annular beam center dark spot ratio by our ingenious design, which has potential implications for constructing compact 3D nonlinear photonic crystal devices.

This work was supported by the Strategic Priority Research Program of the Chinese Academy of Sciences (Grant No. XDA25040201), the National Natural Science Foundation of China (Grant No. 51727901), and the Key Laboratory for Laser Plasmas (Ministry of Education).

AUTHOR DECLARATIONS

Conflict of Interest

The authors have no conflicts to disclose.

Author Contributions

Ruonan Wang: Conceptualization (equal); Data curation (equal); Investigation (equal); Writing – original draft (equal); Writing – review & editing (equal). **Qiang Cao:** Funding acquisition (lead); Project administration (lead); Supervision (lead); Writing – review & editing (equal). **Xiaoliang Wang:** Investigation (equal); Methodology (supporting). **Fengchang Li:** Data curation (equal); Investigation (equal).

DATA AVAILABILITY

The data that support the findings of this study are available from the corresponding author upon reasonable request.

REFERENCES

[1]H. He, M. E. J. Friese, N. R. Heckenberg, and H. R. Dunlop, Phys. Rev. Lett. **75**, 826 (1995).
[2]S. H. Tao, X. C. Yuan, J. Lin, X. Peng, and H. B. Niu, Opt. Express **13**, 7726 (2005).
[3]K. Dholakia and T. Cizmar, Nat. Photonics **5**, 335–342 (2011).
[4]J. Wang, J. Y. Yang, I. M. Fazal, N. Ahmed, Y. Yan, H. Huang, Y. Ren, Y. Yue, S. Dolinar, M. Tur, and A. E. Willner, Nat. Photonics **6**, 488–496 (2012).
[5]A. Mair, A. Vaziri, G. Weihs, and A. Zeilinger, Nature **412**, 313–316 (2001).
[6]R. Fickler, R. Lapkiewicz, W. N. Plick, M. Krenn, C. Schaeff, S. Ramelow, and A. Zeilinger, Science **338**, 640–643 (2012).
[7]L. Allen, M. W. Beijersbergen, R. J. C. Spreeuw, and J. P. Woerdman, Phys. Rev. A **45**, 8185–8189 (1992).
[8]I. V. Basistiy, V. Y. Bazhenov, M. S. Soskin, and M. V. Vasnetsov, Opt. Commun. **103**, 422–428 (1993).
[9]A. Forbes, A. Dudley, and M. McLaren, Adv. Opt. Photonics **8**, 200 (2016).
[10]K. Sueda, G. Miyaji, N. Miyanaga, and M. Nakatsuka, Opt. Express **12**, 3548 (2004).
[11]L. Marrucci, J. Nanophotonics **7**, 078598 (2013).
[12]L. Wang, S. Kruk, K. L. Koshelev, I. I. Kravchenko, B. Lutherdavies, and Y. S. Kivshar, Nano Lett. **18**, 3978 (2018).
[13]N. V. Bloch, K. Shemer, A. Shapira, R. Shiloh, I. Juwiler, and A. Arie, Phys. Rev. Lett. **108**, 233902 (2012).
[14]A. Shapira, I. Juwiler, and A. Arie, Laser Photonics Rev. **7**, L25–L29 (2013).
[15]K. Shemer, N. V. Bloch, A. Shapira, A. Libster, I. Juwiler, and A. Arie, Opt. Lett. **38**, 5470–5473 (2013).
[16]D. Wei, C. Wang, H. Wang, X. Hu, D. Wei, X. Fang, Y. Zhang, D. Wu, Y. Hu, J. Li, S. Zhu, and M. Xiao, Nat. Photonics **12**, 596–600 (2018).
[17]T. Xu, K. Switkowski, X. Chen, S. Liu, K. Koynov, H. Yu, H. Zhang, J. Wang, Y. Sheng, and W. Krolikowski, Nat. Photonics **12**, 591–595 (2018).
[18]X. Xu, T. Wang, P. Chen, C. Zhou, J. Ma, D. Wei, H. Wang, B. Niu, X. Fang, D. Wu, S. Zhu, M. Gu, M. Xiao, and Y. Zhang, Nature **609**, 496–501 (2022).
[19]X. Wang, Q. Cao, R. Wang, X. Cao, and S. Liu, Appl. Phys. Lett. **121**, 181111 (2022).
[20]C. Wang, P. Chen, D. Wei, L. Zhang, Z. Zhang, L. Xu, Y. Hu, J. Li, Y. Zhang, M. Xiao, J. Chu, and D. Wu, ACS Photonics **10**, 456–463 (2023).

[21]S. Liu, L. M. Mazur, W. Krolikowski, and Y. Sheng, Laser Photonics Rev. **14**, 2000224 (2020).
[22]D. Wei, C. Wang, X. Xu, H. Wang, Y. Hu, P. Chen, J. Li, Y. Zhu, C. Xin, X. Hu, Y. Zhang, D. Wu, J. Chu, S. Zhu, and M. Xiao, Nat. Commun. **10**, 4193 (2019).
[23]A. Bahabad and A. Arie, Opt. Express **15**, 17619–17624 (2007).
[24]L. Tian, F. Ye, and X. Chen, Opt. Express **19**, 11591–11596 (2011).
[25]J. Imbrock, L. Wesemann, S. Kroesen, M. Ayoub, and C. Denz, Optica **7**, 28–34 (2020).
[26]S. Liu, L. Wang, L. M. Mazur, K. Switkowski, B. Wang, F. Chen, A. Arie, W. Krolikowski, and Y. Sheng, Adv. Opt. Mater. **11**, 2300021 (2023).
[27]J. Hua, F. Yu, Z. Tian, Y. Yu, and Y. Yu, J. Laser Micro Nanoeng. **12**, 207–211 (2017).
[28]O. Gayer, Z. Sacks, E. Galun, and A. Arie, Appl. Phys. B **91**, 343–348 (2008).
[29]R. Wang, Q. Cao, X. Wang, X. Tian, and F. Li, Opt. Lett. **49**, 1097–1100 (2024).
[30]Y. Sheng, A. Best, H. Butt, W. Krolikowski, A. Arie, and K. Koynov, Opt. Express **18**, 16539–16545 (2010).